Research Square

Preprints are preliminary reports that have not undergone peer review.
They should not be considered conclusive, used to inform clinical practice,
or referenced by the media as validated information.

Electrospun form-stable phase change materials based on fatty acid methyl ester ternary eutectic mixtures and poly(ε-caprolactone) for food packaging applications

Ignacio Solaberrieta
University of Alicante
Soledad Roche
University of Alicante
Cristina Mellinas
University of Alicante
Alfonso Jiménez
University of Alicante
María Carmen Garrigós
mc.garrigos@ua.es

University of Alicante

Research Article

Keywords: Electrospinning, phase change material, fatty acid methyl esters, poly(ε-caprolactone), food packaging

Posted Date: May 14th, 2026

DOI: https://doi.org/10.21203/rs.3.rs-9602358/v1

License: This work is licensed under a Creative Commons Attribution 4.0 International License. Read Full License

Additional Declarations: No competing interests reported.

Abstract

A ternary eutectic mixture of fatty acid methyl esters (FAMEs), composed of methyl myristate (MM), methyl palmitate (MP), and methyl stearate (MS) was optimized using a mixture experimental design. The resulting eutectic mixture (MM:MP:MS, 5:90:5 mass ratio) was subsequently incorporated into electrospun poly(ε-caprolactone) (PCL) fibers to develop form-stable phase change materials (PCMs) for thermal energy storage and thermal regulation applications. The structure and morphology of the fibers was characterized by scanning electron microscopy (SEM), while the successful incorporation of FAMEs into the PCL matrix was confirmed by Fourier transform infrared spectroscopy (FTIR). Thermal stability was investigated by thermogravimetric analysis (TGA), and the thermal storage capacity and reliability were evaluated using differential scanning calorimetry (DSC). Additionally, the thermoregulation performance of the materials was assessed in simulated packaging systems to evaluate their ability to delay temperature rise. In summary, the PCL/FAMEs fibers demonstrated promising potential for their use in food packaging and cold chain logistics or other temperature-sensitive systems, contributing to products extended shelf life and enhanced food safety.

1. Introduction

The rising living standards of modern society have increased the demand for high-quality products, such as fresh fruits, vegetables, dairy and meat. Ensuring product quality and extending shelf life remains a significant challenge. Temperature plays a critical role in food storage, as it is the primary factor influencing the activation of microbial growth and the rate of chemical reactions. Therefore, maintaining proper refrigeration conditions is essential to preserve food quality, safety, and shelf life. Nevertheless, temperature variations during storage and transportation can adversely affect product quality, promoting microbial growth and accelerating chemical reactions such as lipid oxidation, reflected by increased peroxide and thiobarbituric acid values (Karim et al., 2022).

In this context, the development of advanced technologies for cold chain maintenance is a crucial objective (Han et al., 2025). One effective strategy to mitigate these thermal fluctuations is the use of thermal energy storage (TES) systems, which can be implemented through phase change materials (PCMs). PCMs have emerged as promising candidates, as they are capable of absorbing and gradually releasing latent heat during phase transitions, making them increasingly attractive for thermal regulation across various applications, particularly food packaging (Bahrami & Sablani, 2025).

In recent years, latent heat energy storage (LTES) technologies and PCMs have been extensively investigated for thermal regulation applications due to their ability to maintain stable temperatures in a wide range. Numerous reviews have highlighted the relevance of PCMs in this context. For instance, Rozanna et al. (2005) discussed the potential of fatty acids as PCM for thermal energy storage; Yuan et al. (2014) further explored the use of fatty acids in PCM applications; Elias & Stathopoulos, 2019) reviewed various PCM used in thermal energy storage systems; Deka et al. (2026) and Han et al. (2025) examined the recent advances in PCM for food packaging; while Jouhara et al. (2020) provided a comprehensive overview of latent thermal energy storage technologies and their applications.

A proper understanding of the thermal behavior of materials is crucial in the design of LTES systems, especially when using mixtures instead of pure substances such as PCMs. One of the main advantages of using mixtures lies in the potential formation of eutectic compositions, which exhibit sharp phase transitions at specific mass ratios, expanding the range of usable phase change temperatures for different applications (Rubio-Pérez et al., 2021). Among these, fatty acid methyl esters (FAMEs) have gained attention due to their tunable melting points, often slightly above 0°C, and their high latent heat of fusion (> 150 J g^{-1}). In addition to favorable thermal properties such as low vapor pressure and minimal volumetric change during phase transitions, FAMEs offer advantages like chemical stability, non-toxicity, non-flammability, and renewable origin from vegetable or animal oils, making them sustainable and commercially viable options for thermal energy storage (Liston et al., 2016; Wang et al., 2026).

However, molten FAMEs may flow or leak during use. Consequently, they must be placed or encapsulated in specially designed containers or devices, which might raise concerns regarding their thermal resistivity with PCMs. This approach can also increase system costs due to the need for additional storage components. These drawbacks may be addressed by using form-stable PCMs, which maintain shape without additional encapsulation, offer tunable dimensions, and can be processed using different techniques, such as electrospinning (Cai, Ke, et al., 2012; C. Li et al., 2025).

Electrospinning is a simple, versatile and cost-effective technique for producing fibers with controlled structure and dimensions from a wide variety of materials, including both, natural and synthetic polymers (Torres-Giner et al., 2016). The morphology and diameter of the resulting polymeric fibers widely vary depending on several parameters and operating conditions. On the one hand, polymer and solution properties such as polymer concentration, molecular weight, density, viscosity, surface tension and solvent polarity play a critical role. On the other hand, processing conditions including applied voltage, spinneret-to-collector distance, flow rate, inner needle diameter, type of collector, among others, also significantly affect the fiber production process. Moreover, environmental factors, including working temperature and relative humidity, further influence fiber morphology and properties. Therefore, rigorous control of these parameters is essential to ensure process reproducibility and to tailor the final fiber characteristics (Panditkar et al., 2026; Zhang et al., 2020). Due to its versatility, electrospinning has been widely applied to develop functional materials with antioxidant, antimicrobial, and antifungal properties for food packaging (Ren et al., 2025; Solaberrieta et al., 2020; Zhao et al., 2020), textiles (Dejene, 2025), materials for biomedical applications such as wound healing and tissue engineering (Al-Moalemi et al., 2022; Azimi et al., 2020; Mwiiri & Daniels, 2020; Tan et al., 2022), catalysis and filtration (R. Chen et al., 2025), sensors (Cacciotti et al., 2020; Guclu et al., 2023; Kim et al., 2023), and phase change fibers for thermal energy storage (Suárez-García et al., 2023; Wu et al., 2018; Yazdani McCord et al., 2024), among others.

Electrospun fibers have also been extensively employed to develop form-stable PCM materials based on FAMEs and fatty acids, effectively preventing leakage during phase transitions (Gupta et al., 2016; Patel et al., 2023; Xie et al., 2020). For instance, Ke and Li (2017) incorporated several fatty acid esters including ethyl laureate, butyl stearate, ethyl palmitate, ethyl stearate and methyl palmitate as PCMs into electrospun polyacrylonitrile nanofibers, highlighting their potential for applications related to storage and retrieval of thermal energy. Similarly, Onder and Sarier (2020) incorporated methyl palmitate and isopropyl palmitate into electrospun polyacrylonitrile and poly(methacrylic acid-co-ethyl acrylate) fibers, suggesting their suitability

for ambient and cold energy storage in textiles, packaging and medical applications. Cai, Ke, et al. (2012) also reported the fabrication of electrospun form-stable PCMs using binary eutectic mixtures of lauric, myristic, palmitic, and stearic acids in polyethylene terephthalate matrices, which demonstrated promising properties for thermal energy storage applications.

On the other hand, poly(ε-caprolactone) (PCL), a biodegradable and biocompatible polymer, is commonly used in biomedical applications (de Figueiredo et al., 2022; Guleken et al., 2021; Miguel et al., 2017) and food packaging (Dumitriu et al., 2021; Guclu et al., 2023; Opálková Šišková et al., 2022; Salević-Jelić et al., 2024). It offers advantages such as adequate mechanical properties, good thermal stability, and commercial availability. Moreover, PCL has been also used in the development of PCM materials (Baniasadi et al., 2023; Chai et al., 2022; Drago et al., 2023).

In this context, a ternary eutectic mixture composed of methyl palmitate, methyl myristate, and methyl stearate was formulated using a mixture design approach, with the objective of developing a PCL-based PCM suitable for processing via electrospinning, aiming to enhance the thermal management performance in food packaging or other temperature-sensitive systems.

2. Materials and Methods

2.1. Reagents and raw materials

Poly(ε-caprolactone) CapaTM 6800 (PCL, M_w = 80,000 g/mol) was supplied by Perstorp (Malmö, Sweden). Methyl myristate (MM, ≥ 99%), methyl palmitate (MP, ≥ 99%) and methyl stearate (MS, ~ 99%) and dichloromethane (DCM, 99.5%) were purchased from Sigma Aldrich (Madrid, Spain). All chemicals were used as received without any further purification.

2.2. Preparation of ternary FAMEs mixtures

A series of FAMEs mixtures were prepared by heating ultrasonic method according to previous studies with slight modifications (Cai, Ke, et al., 2012; Ke, Li, et al., 2013). Briefly, the individual components were accurately weighed and combined in the appropriate ratios. Then, the FAMEs mixtures were placed in an ultrasonic water bath at 50°C for 30 min to ensure homogenization in the liquid phase. Finally, the mixtures were cooled to room temperature and stored in the dark until further analysis.

2.3. Determination of ternary eutectic FAMEs composition using mixture experimental design

A mixture experimental design based on response surface methodology (RSM) was employed to optimize the composition of the FAMEs ternary mixture, using MP, MM, and MS as individual components. A linear mixture model was fitted to evaluate the influence of each compound on the melting and crystallization enthalpies. RSM is a powerful statistical tool that allows the modelling and optimization of multiple responses influenced by process variables. In the context of mixture experimental designs, it enables the exploration of complex interactions between mixture components while adhering to the constraint that their

proportions must sum to unity (Abed et al., 2023; Duarte et al., 2021; Guimarães et al., 2022; Z. Li et al., 2021).

For this purpose, the mathematical and statistical software Statgraphics Centurion XVI (Statistical Graphics, Rockville, MD, USA), was used to generate the experimental matrix, fit the models, and identify the optimal mixture compositions. MP, MM and MS were treated as independent variables, while the melting and crystallization enthalpies were set as the responses to be maximized. The experimental design consisted of eight mixtures, including three replicated points to improve the robustness and estimation of the model error. The selection of the component composition range was based on preliminary experimental results. All experimental runs were performed randomly to minimize the effect of unexpected variability in the response variables. Separate lineal models were subsequently developed for each selected response. Finally, the analysis of variance (ANOVA) was carried out.

A linear mixture experimental design assumes that the response is a linear function of the components proportions, without considering interaction or higher-order terms. It is particularly useful to estimate the main effects of each component on the response variables. For both, melting and crystallization enthalpies, the experimental data were fitted to Eq. (1).

$$\mathrm{Y} = \beta_1 \mathrm{x}_1 + \beta_2 \mathrm{x}_2 + \beta_3 \mathrm{x}_3$$

1

Where Y is the predicted response and x_1, x_2 and x_3 represent the mass fraction of MP, MM and MS respectively. The coefficients β_1, β_2 and β_3 correspond to the estimated effect of each individual component on the response variable. The suitability of the model to accurately represent the experimental data was assessed using the lack of fit test and the coefficient of determination (R^2). The significance of the model parameters was evaluated at a 5% significance level ($\alpha = 0.05$).

2.4. Preparation of electrospun microfibers

The ternary eutectic FAMEs mixture (MM, MP, MS mass ratio 5:90:5) was prepared by blending the three components at 50 ºC for 30 min under sonication in a glass vial, and after complete homogenization mixtures were stored in the dark until further use. The polymer solution for electrospinning was prepared according to Paroutoglou et al. (2022), with slight modifications. Briefly, PCL (13 wt%) was initially dissolved in dichloromethane (DCM) at room temperature under gently magnetic stirring overnight. Then, the FAMEs mixture was slowly added and stirred for 2 h to ensure a homogeneous solution. Table 1 summarizes the composition and nomenclature of the different solutions. FAMEs were incorporated at 3 concentration levels (50, 75 and 100%) and neat PCL was used as control material. The mass ratio of FAMEs and PCL was calculated respect to the polymer weight.

Table 1
Nomenclature and composition of electrospinning solutions.

Sample	FAMEs[a] (%)	PCL (g)	FAMEs (g)	DCM (g)	Total (g)
PCL	0	2.60	0.00	17.40	20.00
PCL-50% FAMEs	50	2.60	1.30	16.10	20.00
PCL-75% FAMEs	75	2.60	1.95	15.45	20.00
PCL-100% FAMEs	100	2.60	2.60	14.80	20.00

[a]calculated respect to the polymer weight.

The electrospinning process was carried out at room temperature using a Professional Lab Device (Doxa Microfluidics, Málaga, Spain) equipped with a rotatory collector and two syringe pumps installed on a unidirectional sweep motion system. Figure 1 shows the schematic representation of the fiber production process. Each polymer solution was placed in two 10 mL plastic syringes connected to uniaxial spinnerets with 20 G needles (i.d.=0.6 mm). The distance between the needles and the rotating drum collector (l = 20 cm, r = 5 cm) was set to 18 cm. During the electrospinning fiber production process, each spinneret was fed at 1.0 mL h^{-1} and a voltage of 18 kV was applied between the needles and the collector. The rotating speed of the collector was set at 200 rpm, and spinnerets were constantly sweeping between the limits of the drum at a velocity of 20 mm s^{-1}. The electrospinning operation conditions were selected based on preliminary experiments to obtain stable Taylor's cone for fiber production. After the electrospinning process, the obtained mats of fibers were carefully separated from the collector and conveniently stored until further analysis.

2.5. Characterization of electrospun PCL/FAMEs materials

2.5.1. Morphology and structure

The obtained materials were analyzed using scanning electron microscopy (SEM). The fiber mats were mounted on aluminum stubs and coated with a thin layer of gold (≈ 5 nm). The observations were carried out using a SEM JEOL IT500HR/LA (Tokio, Japan). The average fiber diameter (AFD) of each material was calculated using ImageJ software, considering at least 200 random points from the SEM images. The results were reported as mean ± standard deviation and the corresponding histograms were obtained.

2.5.2. Fourier transform infrared spectroscopy (FTIR)

FTIR spectra were obtained using a Jasco FT-IR 4700 IRT-5200 spectrometer (Easton, MD, USA) in the attenuated total reflectance (ATR) mode in the 4000 – 600 cm^{-1} range. Each spectrum was recorded as an average of 64 scans with a spectral resolution of 4 cm^{-1}.

2.5.3. Thermal analysis

Thermal properties of the obtained materials were characterized by thermogravimetric analysis (TGA) and differential scanning calorimetry (DSC). Thermal stability was analyzed with a Mettler Toledo TGA/SDTA

851e equipment (Schwarzenbach, Switzerland). Approximately 5 mg of sample was placed on alumina pans and heated from room temperature to 600 °C at a heating rate of 10 °C min^{-1} under a nitrogen flow of 50 mL min^{-1}. The onset temperature at 5% weight loss ($T_{5\%}$), the temperature corresponding to the maximum degradation rate ($T_{max,i}$; i = 1,2), and the residual mass at 600 °C ($RES_{600°C}$) were determined.

Phase change behavior, including phase transition temperatures and enthalpies, was assessed by DSC using a TA instruments Mod Q2000 calorimeter (New Castle, DE, USA). Approximately 5 mg of sample was placed in closed aluminum pans under nitrogen atmosphere (50 mL min^{-1}). The thermal program consisted of an initial heating step from room temperature to 80 °C, followed by cooling to -20 °C, and a second heating to 80 °C. All stages were performed at 10 °C min^{-1}. The peak maximum was used to determine the melting temperature (T_m) while the corresponding enthalpy (ΔH_m) was calculated based on the peak areas.

Thermal reliability was evaluated by subjecting the PCMs to 100 consecutive heating-cooling cycles between − 20 to 50 °C under nitrogen atmosphere at a heating/cooling rate of 10 °C min^{-1}. Changes in the thermal storage capacity were quantified before and after the 100 cycles. The percentage of variation of melting and crystallization enthalpies was calculated according to Equations (2) and (3):

$$\left|\Delta \varvec{H}_{\varvecm}\varvec{'}\right| = 100\ \frac{\left|\Delta \varvec{H}_{\varvecm,\varvec{a}} - \Delta \varvec{H}_{\varvecm,\varvec{b}}\right|}{\Delta \varvec{H}_{\varvecm,\varvec{b}}}$$

2

$$\left|\Delta \varvec{H}_{\varvecc}\varvec{'}\right| = 100\ \frac{\left|\Delta \varvec{H}_{\varvecc,\varvec{a}} - \Delta \varvec{H}_{\varvecc,\varvec{b}}\right|}{\Delta \varvec{H}_{\varvecc,\varvec{b}}}$$

3

Where $\Delta H_{m,b}$ and $\Delta H_{m,a}$ represent the melting enthalpy of the PCMs before and after 100 cycles, respectively. Likewise, $\Delta H_{c,b}$ and $\Delta H_{c,a}$ represent the melting enthalpy of the PCMs before and after 100 cycles, respectively.

Finally, to further investigate the temperature regulation performance, 2 g of each PCM were wrapped around a temperature data logger to simulate packaging applications. The assembled systems were introduced in sealed bags and preconditioned at 5 °C in a refrigerator for 90 min, then immediately transferred to an incubator maintained at 35 °C for additional 90 min. The temperature profile at the interior of the packaging systems was determined by measuring the temperature at 1-min intervals. Three consecutive heating/cooling cycles were carried out to evaluate the reproducibility of the thermal response. Neat PCL mats were used as control material.

3. Results and Discussion

3.1. Ternary eutectic FAME mixtures composition

Table 2 displays the composition of the ternary FAME mixtures analyzed in the experimental design, along with the corresponding results for the studied responses.

Table 2
Linear mixture experimental design matrix and response variables obtained by DSC of the mass fractions of methyl palmitate (X_{MP}), methyl myristate (X_{MM}) and methyl stearate (X_{MS}).

Mixture	x_{MP} (%)	x_{MM} (%)	x_{MS} (%)	ΔH_m (J g^{-1})	ΔH_c (J g^{-1})
1	90	5	5	198.9	203.5
2	75	20	5	186.5	186.8
3	70	20	10	185.3	184.1
4	75	5	20	184.6	182.0
5	70	10	20	182.2	178.5
6	90	5	5	200.6	204.2
7	75	20	5	190.5	192.0
8	70	20	10	182.8	181.7

The experiment considered three independent variables (mass fractions of MP, MM, and MS). The fusion and crystallization enthalpies (Equations. (4) and (5)), were obtained by fitting the experimental data through multiple regression analysis.

$$\Delta \mathrm{H_m}\left(\mathrm{J\ g^{-1}}\right) = 199.614\mathrm{x_{MP}} + 185.083\mathrm{x_{MM}} + 180.470\mathrm{x_{MS}}$$

4

$$\Delta \mathrm{H_c}\left(\mathrm{J\ g^{-1}}\right) = 203.693\mathrm{x_{MP}} + 185.034\mathrm{x_{MM}} + 175.64\mathrm{x_{MS}}$$

5

Analysis of variance (ANOVA) was performed to evaluate the adequacy and significance of the fitted models for both responses. The calculated linear models adequately fitted the experimental data, as indicated by the high R^2 values (0.9624 and 0.9745 for fusion and crystallization enthalpies, respectively). These models showed no indication of autocorrelation in the residuals (Durbin-Watson > 2), and the standard and mean absolute errors were low, confirming a strong correlation between experimental and predicted values. Therefore, both models can be considered suitable for predicting thermal behavior responses.

The optimization analysis revealed that the same formulation maximized both, the melting and crystallization enthalpies. The optimal mixture consisted of 90% MP, 5% MM, and 5% MS (mass fractions). This composition resulted in the highest thermal energy required for both phase transitions, suggesting a more structured and stable molecular arrangement (Yuan et al., 2014). Furthermore, as shown in Fig. 2, the DSC curves corresponding to this mixture (M1 and M6) exhibited a single, well-defined peak for both

transitions. This behavior differs from the other mixtures, which showed broader and/or multiple peaks, suggesting that the optimal formulation lies within a eutectic composition range. Eutectic systems are characterized by a unique melting point at which all components crystallize simultaneously in a highly organized structure, resulting in sharp thermal peaks (Ke, 2017; Sarı, 2006). This confirms the potential of this mixture for thermal energy storage applications, such as thermal regulation in food packaging (Karim et al., 2022; Shin et al., 2023), offering greater energy storage efficiency due to their well-defined phase transitions and high latent heat values.

3.2. Electrospun PCL/FAMEs PCMs characterization

3.2.1. Morphology and structure of PCL/FAMEs fibers

The electrospinning process successfully produced macroscopically homogeneous, smooth to touch, highly flexible, self-standing, and uniformly white fiber mats in all formulations. Additionally, they exhibited high structural integrity, suggesting good mechanical properties for further applications. In addition, no appreciable leakage was observed for PCL/FAMEs-50% and PCL/FAMEs-75%. However, PCL/FAMEs-100% left a nearly imperceptible trace of FAMEs over a filter paper on the contact points after collection from the electrospinning device. Therefore, this formulation was handled with particular care to minimize possible PCM losses that could otherwise lead to inaccurate results. This observation also suggests that a 100% FAMEs content may be at or slightly above the maximum loading capacity achievable under these processing conditions. To overcome this issue and increase even more the FAMEs content in the materials preventing any leakage, a different approach such as coaxial electrospinning could be considered.

The morphology and diameter distribution of PCL and PCL/FAMEs fibers were characterized by SEM and quantitatively analyzed using image analysis software. Figure 3 presents the SEM micrographs and the corresponding average fiber distributions (AFD) of the electrospun PCMs. Pure PCL fibers displayed a highly heterogeneous diameter distribution, with a significant proportion of fibers measuring under 1 μm, alongside an average fiber diameter of 4.3 ± 1.6 μm, with some fibers even exceeding 10 μm in diameter. Regarding the surface morphology, a porous structure was observed especially in bigger fibers as it is highlighted in the insert of Fig. 3a. This effect was already reported by other authors that also electrospun PCL in organic solvents (TCM, DCM, THF and others) under a wide range of electrospinning processing conditions (Katsogiannis et al., 2015, 2016). According to the literature, the exact mechanism of pore formation depends on several factors. Some authors proposed that ordered arrays of surface pores or breath figures are formed due to the evaporative cooling occurring because of solvent evaporation as the polymer jet is propelled towards the collector. Then, as the surface of the jet cools due to solvent evaporation, water from air condenses on the surface of the fiber. Subsequently, when the fiber dries, water droplets leave an imprint behind (Katsogiannis et al., 2016; Seo et al., 2012). On the other hand, it was also proposed that phase separation could be another possible mechanism for pore formation (Katsogiannis et al., 2015).

As shown in Fig. 3, the incorporation of the FAMEs mixture to the polymer formulations significantly improved the electrospinnability of the polymer solutions and the quality of the fiber mats. Even though fibers with higher average diameters were produced, more homogeneous distributions were observed, which is generally advantageous in terms of mechanical and thermal performance. Uniform fiber diameter

distributions usually help to evenly distribute stress across the whole material, reducing the probability of the formation of weak points that might lead to mechanical failure, while enhancing the structural integrity and durability of the material. From the thermal performance perspective of electrospun phase materials, homogeneous fiber diameters normally lead to more efficient heat transfer and thermal regulation due to a more reliable phase transition behavior (Wu et al., 2018).

In all cases including the FAMEs mixture, the fraction of narrower fibers (around 1 μm) dramatically decreased compared to pure PCL, whereas the AFD increased with the increasing FAMEs content in the polymer mixture. Average diameters of 4.9 ± 1.3 μm, 5.8 ± 1.2 μm, and 5.9 ± 1.1 μm were obtained for PCL/FAMEs-50%, 75% and 100%, respectively. The increase in the AFD with the FAMEs content could be related to the higher viscosity and/or lower conductivity of the mixed solution. C. Chen et al. (2008b) found a similar effect when studying the incorporation of fatty acids on polyethylene terephthalate composite fibers. As shown in Figs. 3b and c, PCL/FAMEs 50% and PCL/FAMEs 75% fibers depicted similar morphologies with relatively smooth cylindrical shape. However, when FAMEs content reached 100% (Fig. 3d) the fibers quality decreased, showing non-uniform and wrinkled surfaces with angles, especially in the axial direction, which might be caused by the aggregation of the excess of FAMEs added to the polymer formulation. Similar results were observed by C. Chen et al. (2008b) and Cai, Ke, et al. (2012) that studied electrospun PCMs based on PET including over 100% mass ratio of fatty acids in their formulations.

3.2.2. FTIR analysis of PCL/FAMEs fibers

The ATR-FTIR spectra of PCL and PCL-FAMEs PCM fibers are shown in Fig. 4. PCL spectra are in close agreement with those reported elsewhere (Rajzer et al., 2019). Asymmetric and symmetric CH_2 stretching bands were observed at 2944 and 2860 cm^{-1}, respectively. The strong signal at 1721 cm^{-1} could be attributed to the ester carbonyl stretching (Bulbul & Dilsiz, 2024). Moreover, the signal observed at 1293 cm^{-1} is related to C-O and C-C backbone vibration in the polyester chain (Miguel et al., 2017). Meanwhile the peaks located at 1238, and 1161 cm^{-1} are ascribed to asymmetric and symmetric C-O-C ester bond vibrations, respectively (Chai et al., 2022; Miguel et al., 2017), while the peak observed at 732 cm^{-1} is usually linked to CH_2 rocking.

On the other hand, the spectra corresponding to the FAMEs mixture (MM:MP:MS mass ratio, 5:90:5) is closely related to the MP spectrum already reported in literature (Alipour et al., 2023; Ke & Li, 2017; Ravotti et al., 2019). The three strong signals located at 2951, 2915 and 2847 cm^{-1} are typically ascribed to asymmetric and symmetric CH_2 vibrations. Peaks at 1736 and 1165 cm^{-1} correspond to the stretching vibrations of C = O and C-O groups of the acyclic saturated ester, respectively (Ke & Li, 2017; Ravotti et al., 2018). Moreover, 1463 and 719 cm^{-1} signals could be associated with the CH_2 or CH_3 deformation vibration and the in-plane rocking vibration in $(-CH_2-)_n$ groups (with $n > 4$) from the aliphatic group in MM, MP and MS (Ke, Li, et al., 2013; Ke & Li, 2017). On the other hand, the band located at 1198 cm^{-1} indicates the tensile vibration motion of the $O-CH_3$ group (Alipour et al., 2023). All strong, moderate and weak bands appearing between 1463 and 719 cm^{-1} could be associated with the scissoring, rocking and twisting vibration of $-CH_2$ groups (Onder & Sarier, 2020).

Compared with the FTIR spectra of pure PCL fibers and the FAMEs mixture, the FTIR spectra of the electrospun PCL/FAMEs PCMs displayed a combination of characteristic signals from both components. This observation confirms the successful incorporation of FAMEs into the fibers during the electrospinning process. In addition, as the concentration of the FAMEs mixture in the electrospinning solution increased, the intensity of the corresponding methyl esters signals became more pronounced, as highlighted in the light-blue areas of Fig. 4, as expected.

3.2.3. Thermal stability of PCL/FAMEs fibers

The thermal stability of pure PCL and the PCL/FAMEs fibers was investigated by TGA under nitrogen atmosphere. The TGA and differential TGA (DTGA) curves were recorded from room temperature to 600 ºC and are shown in Figs. 5a and b, respectively. Characteristic parameters of the thermal degradation processes, including the temperature at 5% weight loss ($T_{5\%}$), the maximum decomposition temperatures ($T_{max,1}$ and $T_{max,2}$) and the char residue at 600 ºC are summarized in Table 3. In all cases, thermal decomposition started at temperatures above 100 ºC, which is significantly beyond the application temperatures expected for these materials in packaging applications. Additionally, the absence of weight loss below 100 ºC confirms that solvent evaporation was complete during the electrospinning process and no solvent remained entrapped within the fiber structure.

Neat PCL fibers decomposed in a single step with an onset decomposition temperature of 367.5 ºC and a temperature of maximum degradation rate of 403.5 ºC. The degradation process extended to approximately 450 ºC resulting in about 99% weight loss. Similarly, the FAMEs sample exhibited a single-step degradation process with an onset temperature of 144.2 ºC, a temperature of maximum degradation rate of 251.4 ºC and complete degradation by 270 ºC attributed to the degradation of the aliphatic chains (Onder & Sarier, 2020).

In contrast, PCL/FAMEs fibers showed a two-step degradation process resulting from the combined thermal behavior of both components. The onset thermal degradation temperature of 5% weight loss in PCL/FAMEs fibers was higher than that of the FAMEs mixture but lower than that of pure PCL fibers, except for the PCL/FAMEs-100% sample, where the higher FAMEs content apparently induced some degree of instability. The first degradation stage occurred approximately between 100 and 270 ºC, showing maximum decomposition temperatures ranging from 199 to 214 ºC, corresponding to the early degradation of FAMEs chains with lower thermal stability. The second stage took place between approximately 350 and 450 ºC with maximum decomposition temperatures around 404 ºC attributed to the degradation of PCL molecular chains.

Furthermore, as illustrated in Fig. 5.a, weight loss during the first thermal degradation step of PCL/FAMEs fibers increased with the FAMEs content in the polymer formulation, as expected. Specifically, the weight loss in the first stage accounted for 34.8%, 43.9% and 50.5 wt% for PCL/FAMEs 50%, 75% and 100%, respectively. This result closely matches the theoretical FAMEs content in the polymer formulations, which were 33.3%, 42.9% and 50.0%, respectively, relative to the total material weight, demonstrating that the FAMEs content in the obtained materials is maintained after the electrospinning process. Moreover, the weight loss related to the second thermal degradation step corresponded to the PCL content in the obtained materials.

Finally, little variations were observed in the char residue at the end of the experiment, ranging from 0.3% to 0.6 wt%. These values are comparable to those of pure PCL samples and this behavior can be attributed to the relatively low molecular weight of the FAMEs compounds, which limit their ability to form char residues at high temperatures.

TGA analyses suggest that PCL/FAMEs fibers possess sufficient thermal stability for their intended application in food packaging materials to reduce temperature variations. Overall, these results agree with previous studies on PCMs based on fatty acid methyl esters (Ma et al., 2022; Onder & Sarier, 2020), fatty acids (Cai, Gao, et al., 2012; Cai, Ke, et al., 2012; Drago et al., 2023; Ke, Cai, et al., 2013; Ke, Li, et al., 2013), polyethylene glycol (Chai et al., 2022), among others, incorporated into polymer matrices.

Table 3
Thermal decomposition parameters of PCL/FAMEs fibers.

Sample	$T_{5\%}$ (°C)	$T_{max,1}$ (°C)	$T_{max,2}$ (°C)	$\%Res_{600°C}$
PCL	367.5	-	403.5	0.3
PCL/FAMEs-50%	157.4	203.2	403.4	0.4
PCL/FAMEs-75%	160.3	214.1	404.0	0.3
PCL/FAMEs-100%	136.5	199.2	404.1	0.6
FAMEs	144.2	251.4	-	0.0

3.2.4. Thermal properties and heat storage capacities of PCL/FAMEs fibers

The practical application of materials designed for thermal regulation are generally governed by their thermal properties, particularly high latent heat and appropriate phase transition temperatures. In this context, DSC was used to characterize the phase change behavior of all materials. The phase transition temperature was determined from the peak point of the DSC thermograms, while the enthalpy associated with the process was calculated from the area under the peak. Figure 6 displays the DSC thermograms corresponding to the second heating cycle of the FAMEs mixture, neat PCL fibers, and PCL/FAMEs fibers with different mass ratios. The main thermal parameters are summarized in Table 4. $T_{m,1}$ and $\Delta H_{m,1}$ represent the melting temperature and enthalpy associated with FAMEs, while $T_{m,2}$ and $\Delta H_{m,2}$ corresponded to those of PCL.

As expected, the FAMEs mixture and neat PCL fibers exhibited single melting transitions at approximately 26.1 ºC and 55.1 ºC, respectively. These findings are consistent with previous studies. Chai et al. (2022) and Drago et al. (2023) reported melting points of 56.4 ºC and 57.0 ºC, respectively, for electrospun PCL-based PCMs.

PCL/FAMEs fibers exhibited two clearly distinguishable thermal transitions. In all formulations, $T_{m,1}$ showed no significant deviation (< 0.2 ºC) from pure FAMEs mixture, indicating that the FAMEs/PCL mass ratio has minimal influence on the phase transition temperature of the FAMEs component. The enthalpy values of PCL/FAMEs fibers with different mass ratio were significantly lower than that of the pure FAMEs mixture.

This reduction is attributed to the fact that PCL does not contribute to the latent heat associated with the phase transition around 26 ºC. Additionally, the DSC thermograms and corresponding ΔH_m values summarized in Table 4, confirmed that the enthalpy associated with the melting transition of the FAMEs mixture decreased as their content in the formulation was reduced, as expected. These results agree with those reported by other authors (Cai, Ke, et al., 2012; Chai et al., 2022).

Table 4
Values of melting temperatures and enthalpy for the FAMEs and PCL/FAMEs fibers.

Sample	FAMEs		PCL	
	$T_{m,1}$(°C)	$\Delta H_{m,1}$ (J g^{-1})	$T_{m,2}$(°C)	$\Delta H_{m,2}$ (J g^{-1})
PCL	-	-	55.1 ± 0.8	58.9 ± 1.6
PCL/FAMEs-50%	26.0 ± 0.5	51.3 ± 1.4	50.1 ± 0.3	41.2 ± 2.1
PCL/FAMEs-75%	26.0 ± 0.3	72.5 ± 3.8	49.7 ± 0.2	36.3 ± 1.8
PCL/FAMEs-100%	25.9 ± 0.2	91.1 ± 3.4	49.5 ± 0.1	32.6 ± 0.8
FAMEs	26.1 ± 0.2	199.8 ± 9.3	-	-

Furthermore, the theoretical enthalpy values of the PCL/FAMEs fibers can be estimated by multiplying the latent heat of the pure FAMEs mixture by its mass fraction within each formulation (C. Chen et al., 2008b, 2008a, 2009; Ke, Cai, et al., 2013; Ke, Li, et al., 2013). Based on this approach, the theoretical enthalpies were calculated and resulted in 66.6, 85.6 and 99.9 J g^{-1} for PCL/FAMEs-50%, PCL/FAMEs-75% and PCL/FAMEs-100% respectively, higher than the experimentally measured melting enthalpy values (Table 4). This effect might be due to the fact that after electrospinning, the crystallization of FAMEs might have been hindered by the quenching effect of the fiber production process and the confinement effect of the PCL matrix. Under these conditions, the FAMEs molecules may not have enough time to form well-ordered crystalline structures due to the rapid evaporation of the solvent during the electrospinning process. Moreover, hydrogen bonding interactions between PCL and FAMEs molecules could contribute to the formation of three-dimensional networks, that, combined with the shield supporting effect provided by the PCL matrix, could substantially restrict molecular mobility during the phase transition processes, resulting in slightly reduced enthalpies compared to the theoretical values (C. Chen et al., 2008b, 2009; Ke, Li, et al., 2013). Regarding the melting transition of the polymer component, a clear decrease in temperature was observed from 55.1 ºC for neat PCL to 50.1, 49.7 and 49.5 ºC, for PCL/FAMEs-50%, PCL/FAMEs-75% and PCL/FAMEs-100%, respectively.

The thermal properties required for PCMs depend on their intended application. The obtained PCL/FAMEs fibers exhibited a thermal transition corresponding to FAMEs melting around 26 ºC, which is close to room temperature in mild to warm climates. Therefore, these materials may be suitable for use in food packaging applications, particularly for maintaining the cold chain preventing temperature rise.

3.2.5. Thermal reliability of PCL/FAMEs fibers

An effective PCM must exhibit both, thermal and chemical stability over a large number of melting and freezing cycles, maintaining its properties for long-term uses. The thermal reliability and reusability of the PCL/FAMEs fibers were evaluated by subjecting the samples to 100 consecutive heating-cooling cycles between − 20 and 50 ºC. Figure 7 depicts the DSC curves of the FAMEs mixture and PCL/FAMEs fibers before and after the thermal cycling, while Table 5 summarizes the corresponding thermal transition parameters.

As shown in Fig. 7 and Table 5, these materials demonstrated excellent thermal stability with no significant changes observed in their melting and crystallization temperatures or enthalpies. After 100 cycles, the melting and crystallization peaks maintained their original shapes, and no major differences were detected in the phase transition behavior throughout the entire process. Only slight variations were observed for the FAMEs mixture and the PCL/FAMEs-50% sample (Figs. 7a and b). Moreover, according to Table 5, both the melting and the crystallization temperatures remained highly consistent before and after thermal cycling, exhibiting no significant shifts. Moreover, the changes in both the melting and crystallization enthalpies were minimal, ranging from 0.06% to 1.54% and from 0.09% to 0.53%, respectively.

This consistency indicates that the fiber structure effectively prevents leakage of the FAMEs mixture during the melting process and preserves the thermal performance of the material. This finding is consistent with previous reports on electrospun PCM systems incorporating FAMEs (Onder & Sarier, 2020), fatty acids (Xie et al., 2020) and others (Chai et al., 2022) in various polymer materials. Furthermore, the minimal variations observed are practically negligible for real applications, highlighting the potential of PCL/FAMEs fibers as promising, highly thermally stable PCMs suitable for repeated long-term use in practical applications.

Table 5
Thermal characteristics of the FAMEs mixture and the PCL/FAMEs fibers before and after 100 thermal cycles.

		Melting process			Freezing process		
Sample	cycle	T_m (ºC)	ΔH_m ($J\ g^{-1}$)	$\lvert\Delta H_m'\rvert$ (%)	T_c (ºC)	ΔH_c ($J\ g^{-1}$)	$\lvert\Delta Hc_c'\rvert$ (%)
PCL/FAMEs-50%	1	26.66	57.64	1.54	18.74	54.85	0.53
	100	26.66	56.75		19.20	54.56	
PCL/FAMEs-75%	1	26.62	77.88	0.06	18.81	75.98	0.21
	100	26.62	77.83		18.81	76.14	
PCL/FAMEs-100%	1	26.57	90.02	0.78	18.36	88.68	0.09
	100	26.58	90.72		18.34	88.76	
FAMEs	1	26.55	209.4	0.10	20.26	204.8	0.24
	100	26.05	209.6		20.38	205.3	

3.2.6. Thermoregulating performance of PCL/FAMEs fibers

The temperature regulation capability of PCMs is perhaps their most important characteristic for thermal management applications. The electrospun PCL/FAMEs fibers play two important roles in delaying temperature rise. First, they function as PCM by absorbing external energy as latent heat, preventing heat from reaching the interior of the container and raising its temperature. Second, they also act as an insulating agent.

The thermoregulating performance of materials naturally depends on the quantity of PCM used in the packaging. In this study, each formulation was weighed in an equal amount of 2 g and were subjected to the same initial temperature. In addition, this performance is also influenced by other factors, including the incubation temperature and the relative position of the PCM within the packaging system. Arjenaki et al. (2019) studied the use of tetradecane as a PCM for meat storage and found that its efficiency in maintaining a low product temperature, starting from refrigeration conditions (4 ºC), was significantly higher when the incubation temperature was only slightly above the melting point of the PCM. In contrast, effectiveness dramatically decreased when the exposure temperature was substantially higher than the melting point. Based on these findings and considering that the FAMEs mixture used in this study showed a melting point around 26.5 ºC, an incubation temperature of 35 ºC was selected for these experiments.

Figure 8 shows the temperature profile inside the simulated packaging as a function of time. At low temperatures, no differences were observed between the performance of PCL/FAMEs fibers compared to neat PCL. Specifically, all the materials reached 15 ºC within 6.7 to 7.9 min of exposure to the incubation temperature. However, as heating progressed, the internal temperature of the simulated packaging system increased at different rates, depending on the materials composition. It was observed that within the melting point range of the FAMEs mixture, the slope of the time-temperature curves corresponding to the PCL/FAMEs fibers clearly decreased compared to that of neat PCL, producing a delayed temperature rise. The temperature profile of neat PCL fibers resulted much faster compared to PCL/FAMEs fibers, showing no resistance to temperature changes apart from the inherent insulating capacity of PCL. A one-stage heating curve without any platform was observed, in agreement with similar studies.

In contrast, the PCL/FAMEs fibers exhibited a distinct temperature plateau during the heating process, which can be clearly associated with the phase transition of FAMEs. In addition, a higher FAMEs content correlated with an enhanced ability to absorb energy as latent heat, leading to a more extended plateau and better temperature maintaining capability. Nevertheless, PCL/FAMEs-100% fibers showed no significant improvement over PCL/FAMEs-75%, likely due to partial leakage of excess FAMEs, as already discussed in section 3.2.1.

This behavior can be explained by the fact that, upon reaching the PCM melting point, the fibers absorb a substantial amount of heat, leading to a reduced temperature slope until the phase transition is completed. In fact, as shown in Fig. 8, the elapsed times to reach 26.5 ºC were 17.4 ± 0.3 min, 25.4 ± 1.6 min, 31.4 ± 0.1 min, and 31.3 ± 0.9 min for neat PCL fibers, PCL/FAMEs-50%, PCL/FAMEs-75%, and PCL/FAMEs-100%, respectively. Thus, a remarkable delay of approximately 14 minutes in reaching 26.5 ºC was achieved for the PCL/FAMEs-75%, and PCL/FAMEs-100% samples during incubation. Even more, it is important to emphasize that this experiment is strongly dependent on the amount of material employed in the packaging system. In this case, these results are really promising because this 14-minute delay in reaching 26.5 ºC was achieved

using only 2 g of PCL/FAMEs fibers, which is significantly lower than the quantities of material typically required for thermal management applications.

4. Conclusion

A ternary eutectic mixture of methyl myristate, methyl palmitate, and methyl stearate (5:90:5 mass ratio) was incorporated into electrospun PCL fibers to develop novel materials with promising characteristics for thermal regulation applications. The incorporation of FAMEs into the polymer mixture enhanced fiber morphology likely due to an increase in viscosity or a decrease in solution conductivity or a combination of both effects, resulting in more homogeneous fiber diameter distributions. Moreover, the AFD increased with higher FAMEs while maintaining adequate fiber morphology, although fiber quality slightly diminished when the FAMEs loading reached 100%. Furthermore, the materials exhibited effective heat storage capacity associated with the FAMEs phase transition near 26 ºC and demonstrated high thermal reliability, showing virtually no change in the response after repeated thermal cycling treatment. In addition, the PCL/FAMEs fibers demonstrated good thermal regulation capability, significantly delaying temperature rise in simulated packaging tests using a relatively small quantity of material. In conclusion, PCL/FAMEs fibers are promising materials with strong potential for applications in food packaging and cold chain logistics contributing to extend shelf life and enhance food safety.

Declarations

Conflicts of interest

Authors declare no conflict of interest.

Funding

Authors express their gratitude to the Spanish Ministry of Science, Innovation and Universities (TED2021-130080B-I00) for financial support of this research.

Author Contribution

I.S. S.R. and C.M performed the overall laboratory conceptualization, formal analysis and Investigation, I.S. wrote the original draft. A.J and M.C.G phelped in the formal analysis and performed validation and Writing - Review & Editing,. A.J. and M.C.G. also performed Project Administration and Funding acquisition.

Data Availability Statement.

Data will be available on request.

References

1. Abed, A., Mojtahedi, A., & Lotfollahi Yaghin, M. (2023). Factorial Mixture Design for Properties Optimization and Modeling of Concrete Composites Incorporated with Acetates as Admixtures. *Sustainability*, *15*(13), 10608. https://doi.org/10.3390/su151310608
2. Alipour, A., Eslami, F., & Sadrameli, S. M. (2023). A novel bio-based phase change material of methyl palmitate and decanoic acid eutectic mixture: Thermodynamic modeling and thermal performance. *Chemical Thermodynamics and Thermal Analysis*, *10*, 100111. https://doi.org/10.1016/j.ctta.2023.100111
3. Al-Moalemi, H. A., Izwan Abd Razak, S., & Bohari, S. P. M. (2022). Electrospun sodium alginate/poly(ethylene oxide) nanofibers for wound healing applications: challenges and future directions. *Cellulose Chemistry and Technology*, *56*(3–4), 251–270. https://doi.org/10.35812/CelluloseChemTechnol.2022.56.23
4. Arjenaki, N. O., Soltanizadeh, N., & Hamdami, N. (2019). Designing an active phase change material package for thermal and qualitative protection of meat. *Food Packaging and Shelf Life*, *21*, 100362. https://doi.org/10.1016/j.fpsl.2019.100362
5. Azimi, B., Maleki, H., Zavagna, L., De la Ossa, J. G., Linari, S., Lazzeri, A., & Danti, S. (2020). Bio-Based Electrospun Fibers for Wound Healing. *Journal of Functional Biomaterials*, *11*(3), 67. https://doi.org/10.3390/jfb11030067
6. Bahrami, S., & Sablani, S. S. (2025). Phase Change Materials in Food Packaging: A Review. *Food and Bioprocess Technology*, *18*(4), 3100–3123. https://doi.org/10.1007/s11947-024-03564-0
7. Baniasadi, H., Madani, M., Seppälä, J., Zimmerman, J. B., & Yazdani, M. R. (2023). Form-stable phase change electrospun nanofibers mat with thermal regulation and biomedical multi-functionalities. *Journal of Energy Storage*, *68*, 107660. https://doi.org/10.1016/j.est.2023.107660
8. Bulbul, Y. E., & Dilsiz, N. (2024). Polycaprolactone-Based Composite Electrospun Nanofibers as Hybrid Biomaterial Systems Containing Hydroxyl- or Carboxylic Acid-Functionalized Multiwall Carbon Nanotubes. *Fibers and Polymers*, *25*(5), 1701–1712. https://doi.org/10.1007/s12221-024-00548-x
9. Cacciotti, I., Pallotto, F., Scognamiglio, V., Moscone, D., & Arduini, F. (2020). Reusable optical multi-plate sensing system for pesticide detection by using electrospun membranes as smart support for acetylcholinesterase immobilisation. *Materials Science and Engineering: C*, *111*, 110744. https://doi.org/10.1016/j.msec.2020.110744
10. Cai, Y., Gao, C., Xu, X., Fu, Z., Fei, X., Zhao, Y., Chen, Q., Liu, X., Wei, Q., He, G., & Fong, H. (2012). Electrospun ultrafine composite fibers consisting of lauric acid and polyamide 6 as form-stable phase change materials for storage and retrieval of solar thermal energy. *Solar Energy Materials and Solar Cells*, *103*, 53–61. https://doi.org/10.1016/j.solmat.2012.04.031
11. Cai, Y., Ke, H., Lin, L., Fei, X., Wei, Q., Song, L., Hu, Y., & Fong, H. (2012). Preparation, morphology and thermal properties of electrospun fatty acid eutectics/polyethylene terephthalate form-stable phase change ultrafine composite fibers for thermal energy storage. *Energy Conversion and Management*, *64*, 245–255. https://doi.org/10.1016/j.enconman.2012.04.018

12. Chai, X., Zhao, T., Yue, J., Yang, J., Zhang, S., Du, J., Zhang, A., & Feng, Z. (2022). Flexible and degradable polycaprolactone based phase change composites for thermal energy management. *Reactive and Functional Polymers*, *181*, 105451. https://doi.org/10.1016/j.reactfunctpolym.2022.105451
13. Chen, C., Wang, L., & Huang, Y. (2008a). A novel shape-stabilized PCM: Electrospun ultrafine fibers based on lauric acid/polyethylene terephthalate composite. *Materials Letters*, *62*(20), 3515–3517. https://doi.org/10.1016/j.matlet.2008.03.034
14. Chen, C., Wang, L., & Huang, Y. (2008b). Morphology and thermal properties of electrospun fatty acids/polyethylene terephthalate composite fibers as novel form-stable phase change materials. *Solar Energy Materials and Solar Cells*, *92*(11), 1382–1387. https://doi.org/10.1016/j.solmat.2008.05.013
15. Chen, C., Wang, L., & Huang, Y. (2009). Ultrafine electrospun fibers based on stearyl stearate/polyethylene terephthalate composite as form stable phase change materials. *Chemical Engineering Journal*, *150*(1), 269–274. https://doi.org/10.1016/j.cej.2009.03.007
16. Chen, R., Wang, Q., Shen, R., Gui, Z., Yan, Y., Tang, M., Chen, Z., Shao, Z., & Zheng, G. (2025). Green and efficient electrospinning of ethyl cellulose-based nanofibrous membrane for high-performance and antibacterial air filtration. *Carbohydrate Polymers*, *366*, 123893. https://doi.org/10.1016/j.carbpol.2025.123893
17. de Figueiredo, A. C., Anaya-Mancipe, J. M., de Barros, A. O. da S., Santos-Oliveira, R., Dias, M. L., & Thiré, R. M. da S. M. (2022). Nanostructured Electrospun Polycaprolactone—Propolis Mats Composed of Different Morphologies for Potential Use in Wound Healing. *Molecules*, *27*(16), 5351. https://doi.org/10.3390/molecules27165351
18. Dejene, B. K. (2025). Natural nanofibers for textile applications: A review on electrospinning of cellulose, chitin, and silk for sustainable functional materials. *International Journal of Biological Macromolecules*, *321*, 146597. https://doi.org/10.1016/j.ijbiomac.2025.146597
19. Deka, H., Naseem, A., Bhansali, A. A., Mabood, M. F., Gangawane, K. M., & Sablani, S. S. (2026). Phase Change Materials-Based Biodegradable Packaging for Perishable Food. *Comprehensive Reviews in Food Science and Food Safety*, *25*(1), e70404. https://doi.org/10.1111/1541-4337.70404
20. Drago, E., Campardelli, R., Barbucci, A., & Perego, P. (2023). Polycaprolactone sub-micrometric fibers optimization for primary packaging loaded with fatty acids as natural phase change materials. *Journal of Food Engineering*, *358*, 111680. https://doi.org/10.1016/j.jfoodeng.2023.111680
21. Duarte, B. P. M., Atkinson, A. C., Granjo, J. F. O., & Oliveira, N. M. C. (2021). Optimal design of mixture experiments for general blending models. *Chemometrics and Intelligent Laboratory Systems*, *217*, 104400. https://doi.org/10.1016/j.chemolab.2021.104400
22. Dumitriu, R. P., Stoleru, E., Mitchell, G. R., Vasile, C., & Brebu, M. (2021). Bioactive Electrospun Fibers of Poly(ε-Caprolactone) Incorporating α-Tocopherol for Food Packaging Applications. *Molecules*, *26*(18), 5498. https://doi.org/10.3390/molecules26185498
23. Elias, C. N., & Stathopoulos, V. N. (2019). A comprehensive review of recent advances in materials aspects of phase change materials in thermal energy storage. *Energy Procedia*, *161*, 385–394. https://doi.org/10.1016/j.egypro.2019.02.101
24. Guclu, N., Duzyer Gebizli, S., & Orhan, M. (2023). Development of polycaprolactone-based electrospun <scp>pH</scp> -sensitive sensors as instant colorimetric indicators for food packaging. *Coloration*

Technology, *139*(5), 527–543. https://doi.org/10.1111/cote.12701

25. Guimarães, T. G. S., Andrade, D. F., Santana, A. P. R., Moser, P., Ferreira, S. S., Menezes, I. M. N. R., Amaral, C. D. B., Oliveira, A., & Gonzalez, M. H. (2022). Mixture design and physicochemical characterization of amino acid-based DEEP eutectic solvents (AADES) for sample preparation prior to elemental analysis. *Journal of Molecular Liquids*, *345*, 117887. https://doi.org/10.1016/j.molliq.2021.117887
26. Guleken, Z., Depciuch, J., Ege, H., İlbay, G., Kalkandelen, C., Ozbeyli, D., Bulut, H., Sener, G., Tarhan, N., & Erdem Kuruca, S. (2021). Spectrochemical and biochemical assay comparison study of the healing effect of the Aloe vera and Hypericum perforatum loaded nanofiber dressings on diabetic wound. *Spectrochimica Acta Part A: Molecular and Biomolecular Spectroscopy*, *254*, 119639. https://doi.org/10.1016/j.saa.2021.119639
27. Gupta, R., Kedia, S., Saurakhiya, N., Sharma, A., & Ranjan, A. (2016). Composite nanofibrous sheets of fatty acids and polymers as thermo-regulating enclosures. *Solar Energy Materials and Solar Cells*, *157*, 676–685. https://doi.org/10.1016/j.solmat.2016.07.033
28. Han, L., Zhang, S., Wright, E., Zheng, X., & Yan, Y. (2025). An extensive analysis of the utilisation of phase change materials in food storage process. *Journal of Energy Storage*, *111*, 115391. https://doi.org/10.1016/j.est.2025.115391
29. Jouhara, H., Żabnieńska-Góra, A., Khordehgah, N., Ahmad, D., & Lipinski, T. (2020). Latent thermal energy storage technologies and applications: A review. *International Journal of Thermofluids*, *5–6*, 100039. https://doi.org/10.1016/j.ijft.2020.100039
30. Karim, M., Fathi, M., Soleimanian-Zad, S., & Spigno, G. (2022). Development of sausage packaging with zein nanofibers containing tetradecane produced via needle-less electrospinning method. *Food Packaging and Shelf Life*, *33*, 100911. https://doi.org/10.1016/j.fpsl.2022.100911
31. Katsogiannis, K. A. G., Vladisavljević, G. T., & Georgiadou, S. (2015). Porous electrospun polycaprolactone (PCL) fibres by phase separation. *European Polymer Journal*, *69*, 284–295. https://doi.org/10.1016/j.eurpolymj.2015.01.028
32. Katsogiannis, K. A. G., Vladisavljević, G. T., & Georgiadou, S. (2016). Porous electrospun polycaprolactone fibers: Effect of process parameters. *Journal of Polymer Science Part B: Polymer Physics*, *54*(18), 1878–1888. https://doi.org/10.1002/polb.24090
33. Ke, H. (2017). Phase diagrams, eutectic mass ratios and thermal energy storage properties of multiple fatty acid eutectics as novel solid-liquid phase change materials for storage and retrieval of thermal energy. *Applied Thermal Engineering*, *113*, 1319–1331. https://doi.org/10.1016/j.applthermaleng.2016.11.158
34. Ke, H., Cai, Y., Wei, Q., Xiao, Y., Dong, J., Hu, Y., Song, L., He, G., Zhao, Y., & Fong, H. (2013). Electrospun ultrafine composite fibers of binary fatty acid eutectics and polyethylene terephthalate as innovative form-stable phase change materials for storage and retrieval of thermal energy. *International Journal of Energy Research*, *37*(6), 657–664. https://doi.org/10.1002/er.2888
35. Ke, H., Li, D., Zhang, H., Wang, X., Cai, Y., Huang, F., & Wei, Q. (2013). Electrospun form-stable phase change composite nanofibers consisting of capric acid-based binary fatty acid eutectics and polyethylene terephthalate. *Fibers and Polymers*, *14*(1), 89–99. https://doi.org/10.1007/s12221-013-0089-4

36. Ke, H., & Li, Y. (2017). A series of electrospun fatty acid ester/polyacrylonitrile phase change composite nanofibers as novel form-stable phase change materials for storage and retrieval of thermal energy. *Textile Research Journal*, *87*(19), 2314–2322. https://doi.org/10.1177/0040517516669078
37. Kim, S. W., Kim, E. S., Park, B. J., Jung, Y. W., Kim, D. H., & Lee, S. J. (2023). Polycaprolactone/Anthocyanin-Based Electrospun Volatile Amines Gas Indicator with Improved Visibility by Varying Bi-Solvent Ratio: A Case of Intelligent Packaging of Mackerel. *Foods*, *12*(20), 3850. https://doi.org/10.3390/foods12203850
38. Li, C., Zhang, H., Hu, W., & Wang, G. (2025). Improved energy storage performance through the composition of molecular solar thermal (MOST) molecule and phase change material (PCM) in electrospinning fiber. *Journal of Materials Science*, *60*(2), 706–715. https://doi.org/10.1007/s10853-024-10563-1
39. Li, Z., Lu, D., & Gao, X. (2021). Optimization of mixture proportions by statistical experimental design using response surface method - A review. *Journal of Building Engineering*, *36*, 102101. https://doi.org/10.1016/j.jobe.2020.102101
40. Liston, L. C., Farnam, Y., Krafcik, M., Weiss, J., Erk, K., & Tao, B. Y. (2016). Binary mixtures of fatty acid methyl esters as phase change materials for low temperature applications. *Applied Thermal Engineering*, *96*, 501–507. https://doi.org/10.1016/j.applthermaleng.2015.11.007
41. Ma, J., Liu, H., Sun, D., Wang, J., & Cui, S. (2022). Synthesis of phase change microcapsules with binary fatty acid ester core and their feasibility investigation in energy conservation of cementitious materials. *Construction and Building Materials*, *330*, 127212. https://doi.org/10.1016/j.conbuildmat.2022.127212
42. Miguel, S., Ribeiro, M., Coutinho, P., & Correia, I. (2017). Electrospun Polycaprolactone/Aloe Vera_Chitosan Nanofibrous Asymmetric Membranes Aimed for Wound Healing Applications. *Polymers*, *9*(5), 183. https://doi.org/10.3390/polym9050183
43. Mwiiri, F. K., & Daniels, R. (2020). Electrospun nanofibers for biomedical applications. In *Delivery of Drugs* (pp. 53–74). Elsevier. https://doi.org/10.1016/B978-0-12-817776-1.00003-1
44. Onder, E., & Sarier, N. (2020). Fatty acid alkyl ester nanowebs suitable for renewable thermal energy storage. *Thermochimica Acta*, *690*, 178698. https://doi.org/10.1016/j.tca.2020.178698
45. Opálková Šišková, A., Mosnáčková, K., Musioł, M., Opálek, A., Bučková, M., Rychter, P., & Eckstein Andicsová, A. (2022). Electrospun Nisin-Loaded Poly(ε-caprolactone)-Based Active Food Packaging. *Materials*, *15*(13), 4540. https://doi.org/10.3390/ma15134540
46. Panditkar, S. S., Gurnule, W. B., Waghe, P. U., Gurnule, P. W., & Kumar, P. (2026). The art and science of electrospinning: a detailed review of process and potential applications. *Polymer Bulletin*, *83*(2), 53. https://doi.org/10.1007/s00289-025-06071-0
47. Paroutoglou, E., Fojan, P., Gurevich, L., & Afshari, A. (2022). Thermal Properties of Novel Phase-Change Materials Based on Tamanu and Coconut Oil Encapsulated in Electrospun Fiber Matrices. *Sustainability*, *14*(12), 7432. https://doi.org/10.3390/su14127432
48. Patel, D., Wei, W., Singh, H., Xu, K., Beck, C., Wildy, M., Schossig, J., Hu, X., Hyun, D. C., Chen, W., & Lu, P. (2023). Efficient and Secure Encapsulation of a Natural Phase Change Material in Nanofibers Using Coaxial Electrospinning for Sustainable Thermal Energy Storage. *ACS Sustainable Chemistry & Engineering*, *11*(31), 11570–11579. https://doi.org/10.1021/acssuschemeng.3c02094

49. Rajzer, I., Dziadek, M., Kurowska, A., Cholewa-Kowalska, K., Ziąbka, M., Menaszek, E., & Douglas, T. E. L. (2019). Electrospun polycaprolactone membranes with Zn-doped bioglass for nasal tissues treatment. *Journal of Materials Science: Materials in Medicine*, *30*(7), 80. https://doi.org/10.1007/s10856-019-6280-4
50. Ravotti, R., Fellmann, O., Lardon, N., Fischer, L. J., Stamatiou, A., & Worlitschek, J. (2018). Synthesis and Investigation of Thermal Properties of Highly Pure Carboxylic Fatty Esters to Be Used as PCM. *Applied Sciences*, *8*(7), 1069. https://doi.org/10.3390/app8071069
51. Ravotti, R., Fellmann, O., Lardon, N., Fischer, L. J., Stamatiou, A., & Worlitschek, J. (2019). Analysis of Bio-Based Fatty Esters PCM's Thermal Properties and Investigation of Trends in Relation to Chemical Structures. *Applied Sciences*, *9*(2), 225. https://doi.org/10.3390/app9020225
52. Ren, R., Li, H., Li, M., Gao, Z., Li, S., Wang, H., & Liu, Q. (2025). Citric acid in-situ cross-linked emulsion electrospinning nanofibers based on polyvinyl alcohol and oregano essential oil for food active packaging. *Journal of Materials Science 2025 60:33*, *60*(33), 14800–14819. https://doi.org/10.1007/S10853-025-11323-5
53. Rozanna, D., Chuah, T. G., Salmiah, A., Choong, T. S. Y., & Sa'ari, M. (2005). Fatty Acids as Phase Change Materials (PCMs) for Thermal Energy Storage: A Review. *International Journal of Green Energy*, *1*(4), 495–513. https://doi.org/10.1081/GE-200038722
54. Rubio-Pérez, G., Muñoz-Rujas, N., Aguilar, F., Ravotti, R., Müller, L., & Montero, E. (2021). Evolution of the Study of Phase Diagram of Binary and Ternary Mixtures Involving Fatty Acid Esters. *Materials*, *14*(2), 369. https://doi.org/10.3390/ma14020369
55. Salević-Jelić, A., Lević, S., Prieto, C., Jeremić, S., Stevanović, S., Rac, V., Vukašinović, I., Nedović, V., & Lagaron, J. M. (2024). Polycaprolactone-based electrospun films incorporating sage extract: From active food packaging application to accelerated biodegradation by Pseudomonas. *Future Foods*, *10*, 100465. https://doi.org/10.1016/j.fufo.2024.100465
56. Sarı, A. (2006). Eutectic mixtures of some fatty acids for latent heat storage: Thermal properties and thermal reliability with respect to thermal cycling. *Energy Conversion and Management*, *47*, 1207–1221. https://doi.org/10.1016/j.enconman.2005.07.005
57. Seo, Y.-A., Pant, H. R., Nirmala, R., Lee, J.-H., Song, K. G., & Kim, H. Y. (2012). Fabrication of highly porous poly (ε-caprolactone) microfibers via electrospinning. *Journal of Porous Materials*, *19*, 217–223. https://doi.org/10.1007/s10934-011-9463-z
58. Shin, H., Thanakkasaranee, S., Kambiz, S., & Seo, J. (2023). Preparation and applicability of polylactic acid/polyethylene glycol/nanoclay composite films for smart steam release in microwave packaging. *Food Packaging and Shelf Life*, *40*, 101188. https://doi.org/10.1016/j.fpsl.2023.101188
59. Solaberrieta, I., Jiménez, A., Cacciotti, I., & Garrigós, M. C. (2020). Encapsulation of Bioactive Compounds from *Aloe Vera* Agrowastes in Electrospun Poly (Ethylene Oxide) Nanofibers. *Polymers*, *12*(6), 1323. https://doi.org/10.3390/polym12061323
60. Suárez-García, A., Arce, E., Alford, L., & Luhrs, C. C. (2023). Electrospun composite fibers containing organic phase change materials for thermo-regulation: Trends. *Renewable and Sustainable Energy Reviews*, *187*, 113648. https://doi.org/10.1016/j.rser.2023.113648

61. Tan, G., Wang, L., Pan, W., & Chen, K. (2022). Polysaccharide Electrospun Nanofibers for Wound Healing Applications. *International Journal of Nanomedicine*, *17*, 3913–3931. https://doi.org/10.2147/IJN.S371900
62. Torres-Giner, S., Pérez-Masiá, R., & Lagaron, J. M. (2016). A review on electrospun polymer nanostructures as advanced bioactive platforms. *Polymer Engineering & Science*, *56*(5), 500–527. https://doi.org/10.1002/pen.24274
63. Wang, X., Fu, Y., Washburn, S., Nguyen, T. B., Chauhan, A., Shaikh, S., Zhao, W., Wang, H., & Shi, S. Q. (2026). Fatty acid from recycled waste cooking oil as a phase-change material for thermal storage systems. *RSC Advances*, *16*(7), 5852–5863. https://doi.org/10.1039/D5RA07469J
64. Wu, Y., Chen, C., Jia, Y., Wu, J., Huang, Y., & Wang, L. (2018). Review on electrospun ultrafine phase change fibers (PCFs) for thermal energy storage. *Applied Energy*, *210*, 167–181. https://doi.org/10.1016/j.apenergy.2017.11.001
65. Xie, N., Niu, J., Gao, X., Fang, Y., & Zhang, Z. (2020). Fabrication and characterization of electrospun fatty acid form-stable phase change materials in the presence of copper nanoparticles. *International Journal of Energy Research*, *44*(11), 8567–8577. https://doi.org/10.1002/er.5543
66. Yazdani McCord, M. R., Zimmerman, J. B., & Rojas, O. J. (2024). Harnessing multifunctional electrospun nanofibers containing phase change materials for energy-efficient thermal management: A review on recent trends. *Nano Energy*, *131*, 110212. https://doi.org/10.1016/j.nanoen.2024.110212
67. Yuan, Y., Zhang, N., Tao, W., Cao, X., & He, Y. (2014). Fatty acids as phase change materials: A review. *Renewable and Sustainable Energy Reviews*, *29*, 482–498. https://doi.org/10.1016/j.rser.2013.08.107
68. Zhang, C., Li, Y., Wang, P., & Zhang, H. (2020). Electrospinning of nanofibers: Potentials and perspectives for active food packaging. *Comprehensive Reviews in Food Science and Food Safety*, *19*(2), 479–502. https://doi.org/10.1111/1541-4337.12536
69. Zhao, L., Duan, G., Zhang, G., Yang, H., He, S., & Jiang, S. (2020). Electrospun Functional Materials toward Food Packaging Applications: A Review. *Nanomaterials*, *10*(1), 150. https://doi.org/10.3390/nano10010150

Figures

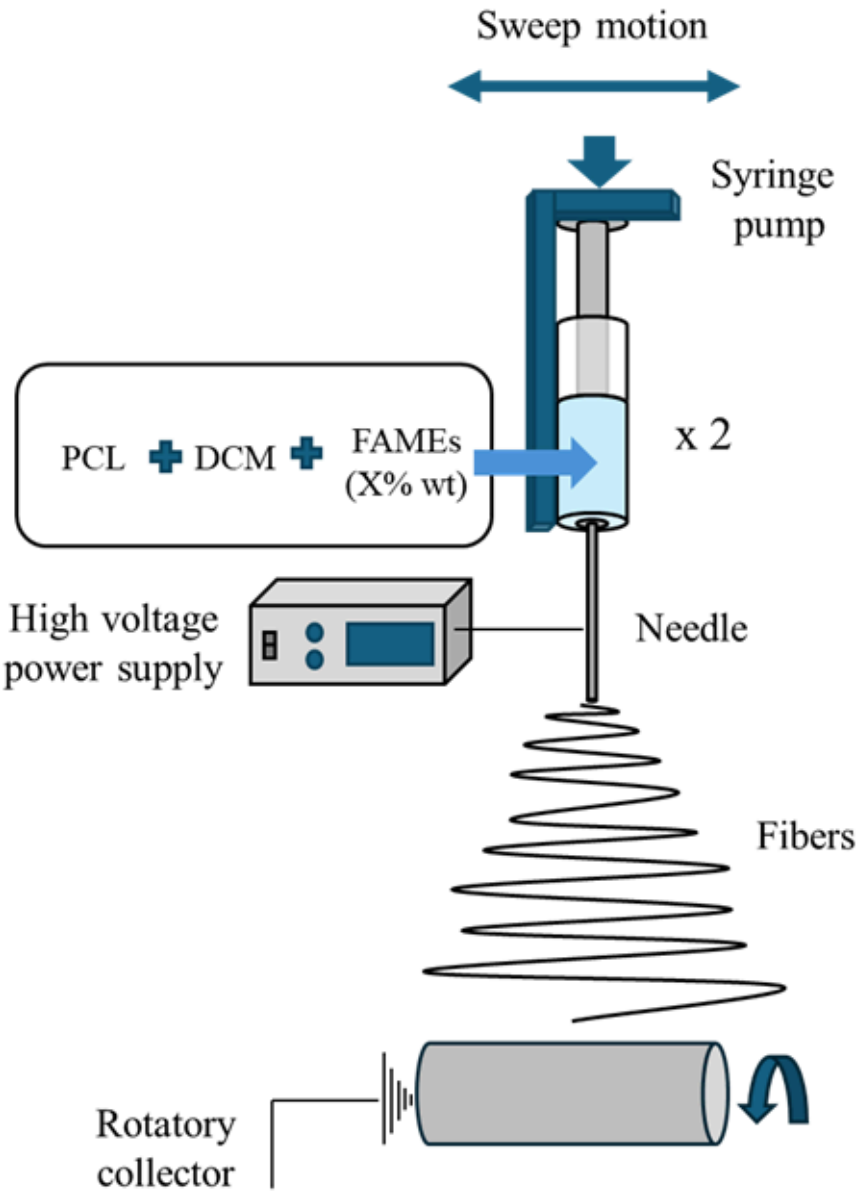


Figure 1

Schematic illustration of the device used for electrospinning

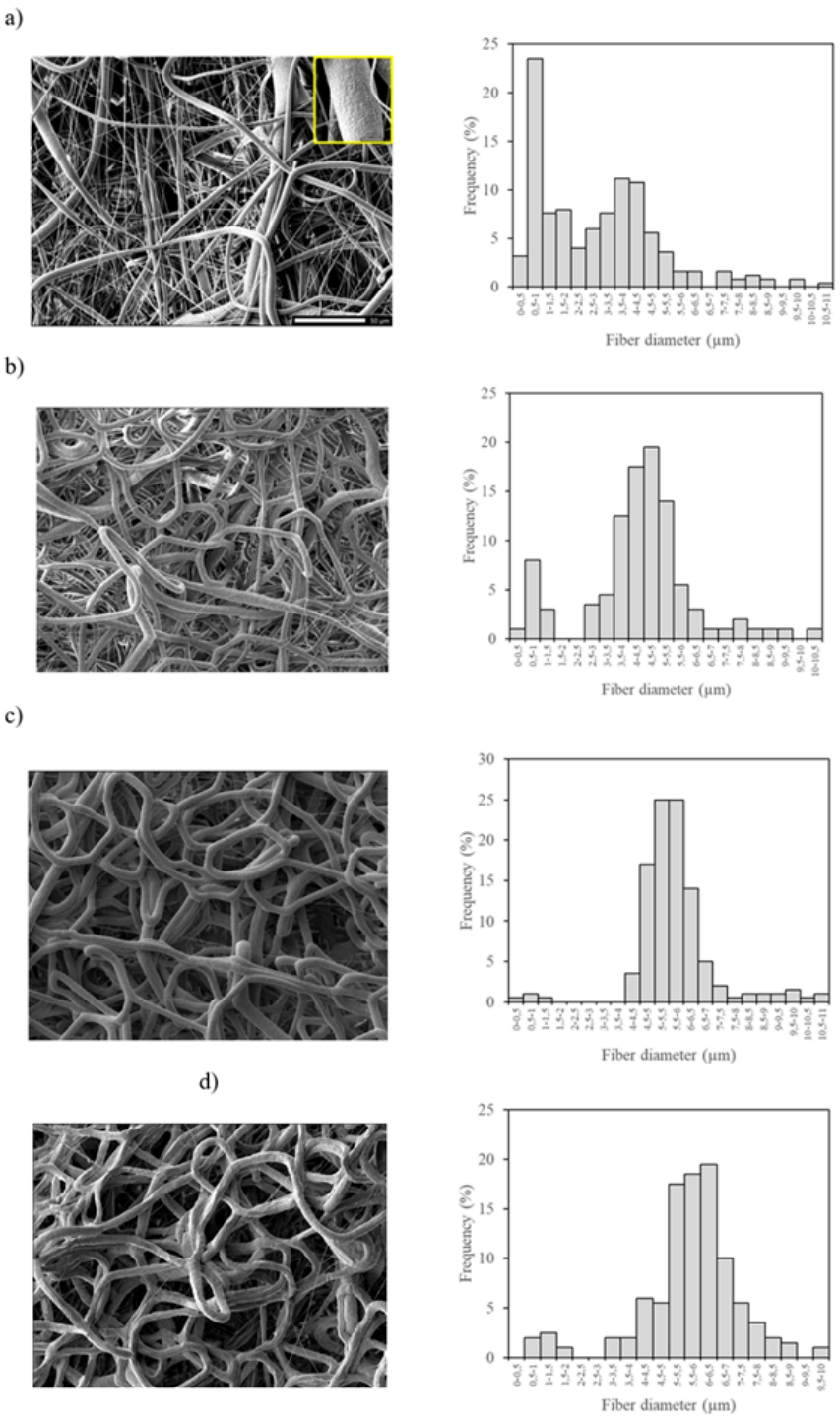


Figure 2

DSC curves of different ternary FAMEs mixtures

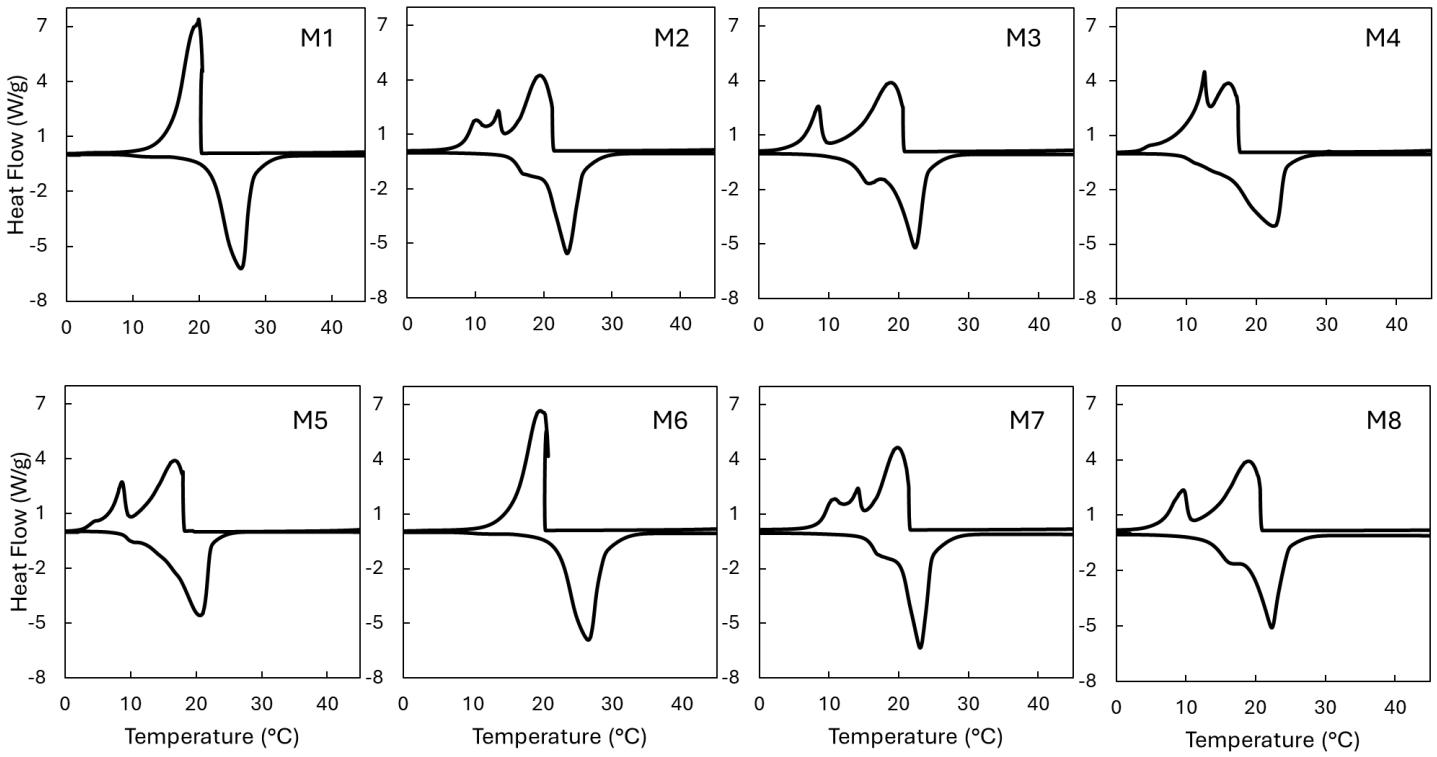


Figure 3

SEM micrographs and diameter distribution of PCL/FAMEs microfibers. a) PCL; b) PCL/FAMEs-50%; c) PCL/FAMEs-75%; d) PCL/FAMEs-100%

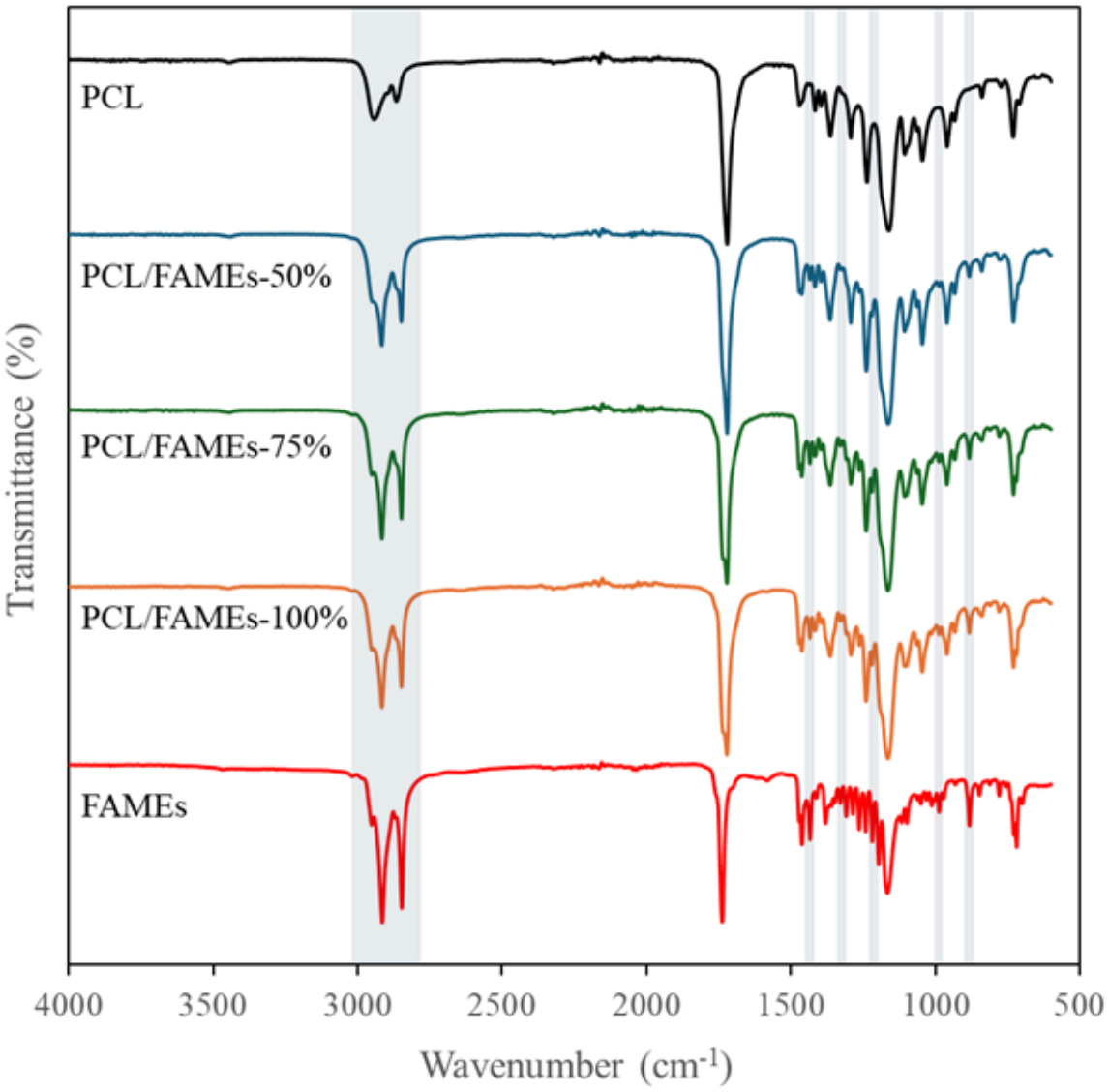
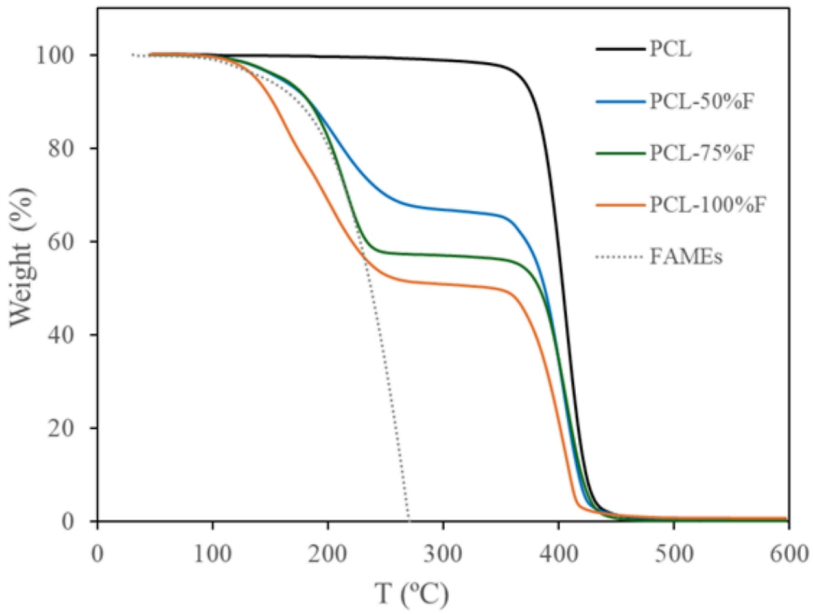


Figure 4

FTIR spectra of PCL, FAMEs and various PCL/FAMEs fibers

a)



b)

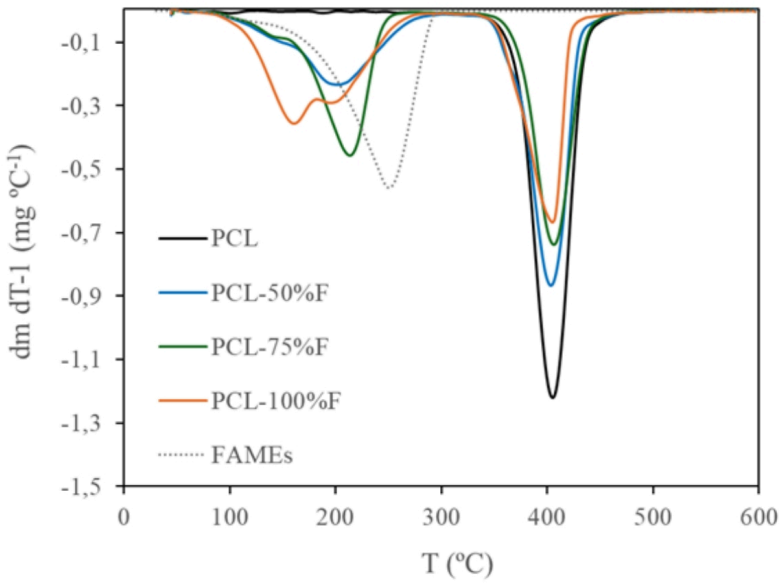


Figure 5

a) TGA and b) DTGA curves of PCL, FAMEs and PCL/FAMEs fibers

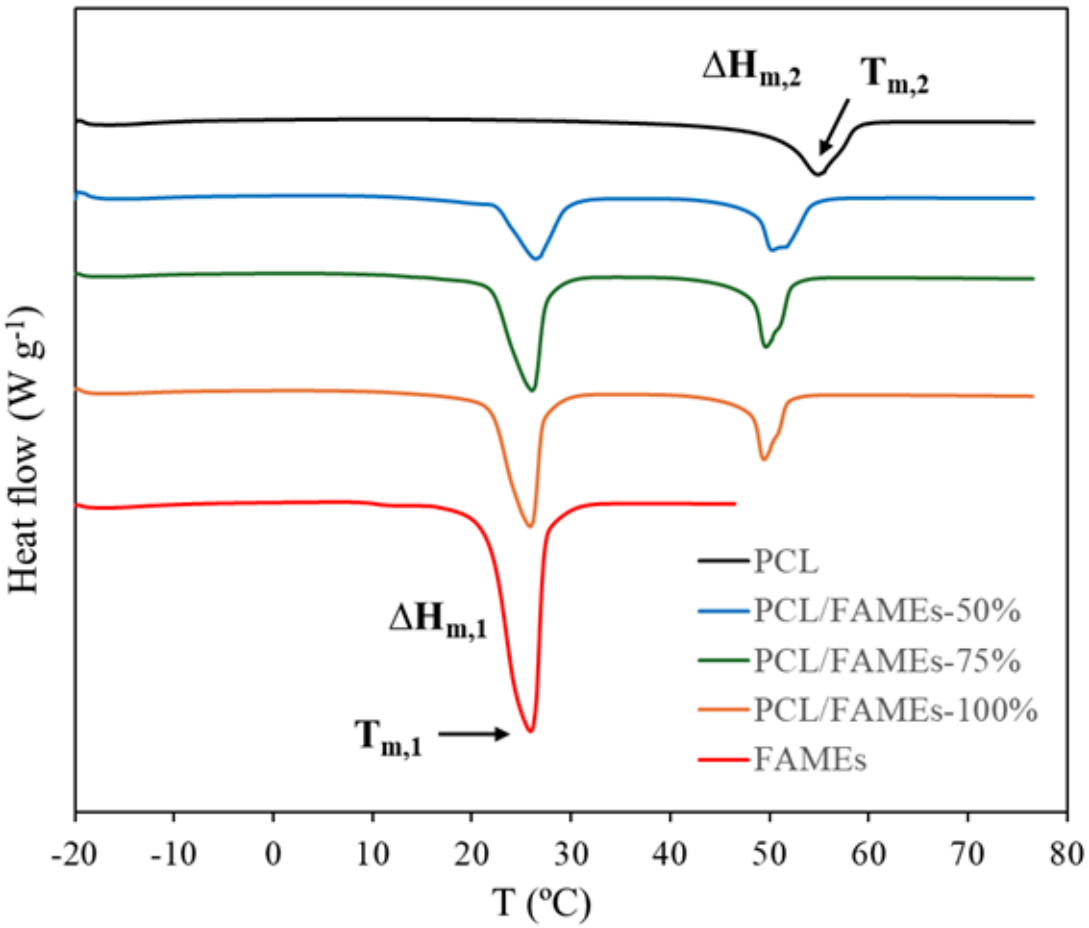


Figure 6

DSC thermograms of FAMEs and PCL/FAMEs fibers. Exo up

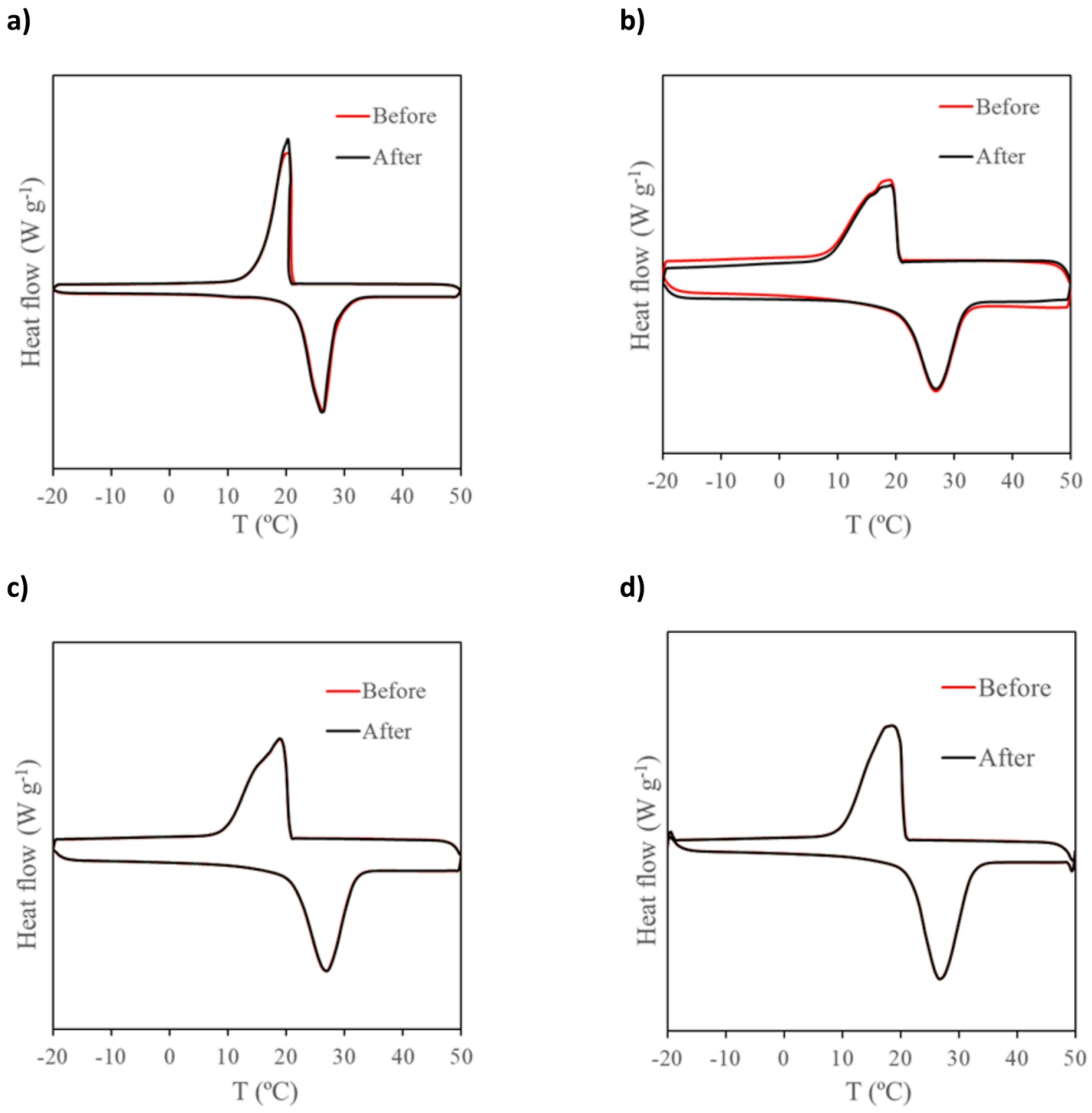


Figure 7

DSC curves of PCL/FAMEs microfibers before and after 100 thermal cycles. a) FAMEs; b) PCL/FAMEs-50%; c) PCL/FAMEs-75%; d) PCL/FAMEs-100%. Exo up

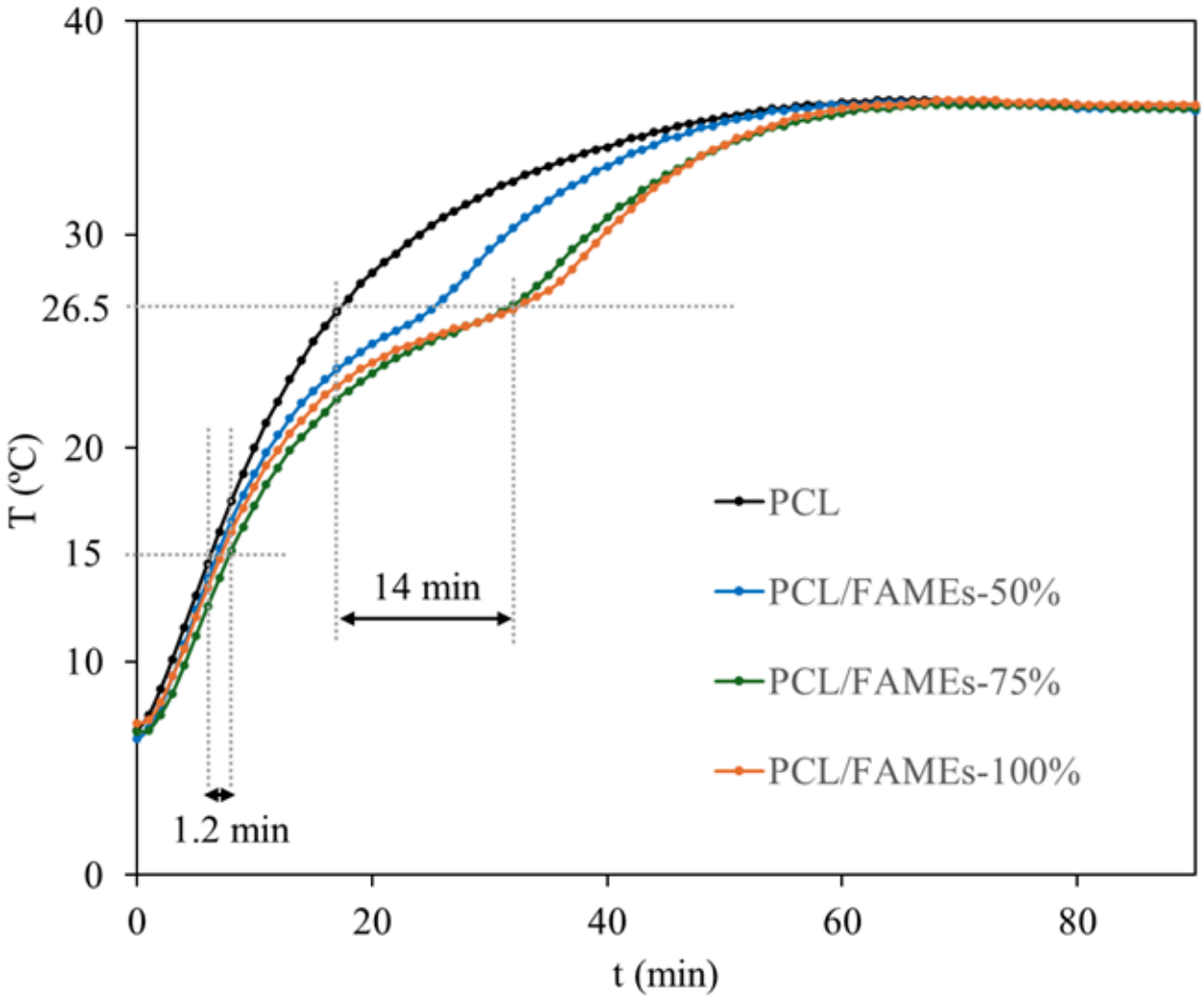


Figure 8

Heating temperature profiles as a function of time for simulated packaging systems using PCL, PCL/FAMEs-50%, PCL/FAMEs-75% and PCL/FAMEs-100% fibers